ISSN 1330-3651 (Print), ISSN 1848-6339 (Online) https://doi.org/10.17559/TV-20240302001362
Original scientific paper

Infrared Image Segmentation Method Based on Variable Helix Optimized-Sparrow Search Algorithm

JiLan HUANG*, Xing YANG, ZhiXiong JIN

Abstract: This study proposes an infrared image segmentation method based on a Variable Helix Optimized-Sparrow Search Algorithm (VHO-SSA) to address the limitations of traditional image segmentation algorithms. The proposed method combines the Otsu threshold algorithm with an optimized sparrow search algorithm, which utilizes a variable helix position search method and a best point set method. The performance of the proposed method is evaluated using several benchmark functions and compared with other state-of-the-art algorithms. The results demonstrate that the VHO-SSA achieves high segmentation accuracy (up to 0.98) and maintains a high structural similarity index (above 0.90) in the presence of noise. The proposed method shows promise for improving the segmentation of infrared images in various applications.

Keywords: division; image; otsu; sparrow search algorithm; threshold; variable helix

1 INTRODUCTION

In the field of digital image processing, image segmentation has been broadly utilized in multiple fields such as security monitoring, remote sensing imaging, clinical medicine, etc. [1]. There are three challenges in infrared image segmentation. First of all, infrared images often have complex backgrounds and contain various noises and disturbances. Second, infrared images usually have low contrast and limited dynamic range, which makes it difficult for threshold-based segmentation methods to distinguish foreground and background. Finally, in some applications, such as security monitoring or medical diagnosis, infrared image segmentation needs to be fast and accurate, and traditional segmentation algorithms often struggle to meet these requirements. At present, the importance of infrared image segmentation is mainly reflected in security monitoring, medical disease diagnosis, industrial fault detection and other fields [2]. At the growth of technology, there is an increasing demand for the efficiency and accuracy of image segmentation algorithms, especially when dealing with infrared images in complex environments. Traditional image segmentation algorithms often perform poorly in the face of noise interference, high dynamic range, and low contrast, which prompts researchers to explore more efficient algorithms. For example, although threshold method is widely used in automatic threshold setting, it performs poorly in noisy environment and is prone to missegmentation, which greatly reduces the effect of image segmentation [3]. Edge detection methods may not be able to accurately identify edges because the method relies on significant grayscale changes [4]. There are also some segmentation methods based on graph theory; although they can provide accurate segmentation results, their computational complexity is high, and they are not suitable for real-time or large-scale applications [5]. In recent years, optimization algorithms based on natural inspiration, such as genetic algorithms, particle swarm optimization algorithms, etc., have shown their unique advantages in the field of image processing. Sparrow Search Algorithm (SSA), as a new type of swarm intelligence optimization algorithm, has been broadly utilized in multiple fields due to its simple and efficient characteristics. However, traditional SSA still has limitations in handling complex image segmentation tasks, such as insufficient search ability in multimodal functions and noise suppression. This study aims to develop a new infrared image segmentation algorithm by introducing the Sparrow search algorithm with variable spiral optimization (VHO-SSA) to solve the problems of noise interference, high dynamic range and low contrast faced by traditional image segmentation algorithms in infrared image processing. There are two novel contributions in this study. The first is the variable spiral optimization strategy. The variable spiral position search method is applied to the Sparrow search algorithm for the first time to improve its search ability and convergence speed in complex image segmentation tasks. The second is the optimization of the best point set. The optimal point set method is used to optimize the initial population distribution, which significantly improves the global search capability and the diversity of the algorithm in multi-peak environment. This study contents include five parts. The first part is an introduction to the entire article, the second part is an analysis and summary of relevant research by others, the third part is an introduction to the algorithm, the fourth part is a performance test of the algorithm, and the fifth part is a summary of the entire article.

2 RELATED WORK

In digital image processing, image segmentation is a very important issue. Many scholars have conducted extensive research on image segmentation techniques and their optimization methods. Luo S. et al. proposed a new convex representation calculation method in image segmentation processing and proved that shape convexity is equivalent to quadratic constraints of related index functions. Research improved probability-based models through this method to extract convex prior targets from images. The superiority of this method has been verified through image segmentation experiments [6]. By improving the training labels in this way, it aims to enhance the effectiveness of image segmentation in real-world applications. Tests on real datasets have found that this method has better classification accuracy than other similar methods [7]. Shuang Q et al. classified image segmentation techniques based on complex modules into two categories

based on the encoding and decoding methods of multimodal information. After organizing the commonly used datasets and evaluation indicators for image segmentation, the performance differences of different types of image segmentation algorithms were compared by applying them. Through a comprehensive analysis of existing image segmentation algorithms, this study provided a reference for the existing shortcomings and future development directions in the field of image segmentation [8]. Xian S. et al. utilized a bias corrected fuzzy mean model to improve image noise resistance and edge recognition performance. The study first utilized the fuzzy mean algorithm of T-sphere to transform digital images into fuzzy sets. Then, the membership degree of the image was calculated, and a new weighting method was used to integrate spatial information. Experiments on 3D image segmentation datasets have shown that this method has reliable accuracy and is superior to similar algorithms [9].

Because of good search ability, SSA has been broadly applied in different fields. Zhang L. et al. observed the homochromatic aberration in color reproduction. Backpropagation neural network (BPNN) was optimized to rebuild spectral reflectance and minimize errors. Besides, a new SSA has been proposed to minimize the impact of original values on BPNN and raise search accuracy. Firstly, it initialized BPNN with SSA, and then sine chaotic mapping was utilized. Finally, compared to other methods, this method has more stable effectiveness and can rebuild spectral reflectance [10]. Zhang S. et al. observed that the patterns' imaging effectiveness is influenced by the projection optical devices' distortion. Thus, on the ground of SSA, a method was put forward for raising the aberration coefficients' distribution. Firstly, it utilized SSA's independence to get an optimized aberration, and then the outcomes were compared with the algorithm. The experiment findings indicated that the improved aberration was better than the outcomes under satisfying status [11]. Hui X. et al. utilized a SSA to constrain hypersonic re-entry trajectories. The control parameters' sensitivity was cut down through optimizing SSA, leading to better initial values. The findings denoted that the calculation algorithm has quick convergence and good robustness [12]. Liu T. et al. raised an assistive system for brain tumor detection. Preprocessing, classification, extraction, and diagnosis are contained in the system. Besides, it optimized the system's search capability with SSA. The outcomes indicated that in contrast to the newest technology, this method was more efficient [13].

In summary, although existing segmentation methods such as threshold method are computationally simple and efficient, they are prone to missegmentation under conditions of high noise level or low image contrast, and particle swarm optimization algorithm, although showing good global search ability in multi-parameter optimization problems, has a slow convergence speed in high-dimensional space and is easy to fall into local optimization. Based on this, the VHO-SSA proposed in this study aims to further improve the adaptability and robustness of the algorithm in complex image segmentation scenarios by introducing a variable spiral position search strategy. By dynamically adjusting the search path, the variable spiral mechanism can avoid the local optimal problem of traditional SSA algorithm more effectively, and accelerate the convergence speed in complex environment. In addition, VHO-SSA can more effectively maintain the stability and segmentation accuracy of the algorithm when processing low contrast and high noise images, thus providing more reliable results in critical applications such as medical imaging and remote sensing images.

3 INFRARED IMAGE SEGMENTATION METHOD BASED ON IMPROVED SPARROW SEARCH ALGORITHM

Infrared image segmentation (IIS) is an important research direction in the field of image processing, especially in infrared imaging technology. Currently, the accurate segmentation of fault areas in infrared images is a challenge due to factors such as background complexity, varying brightness, and low resolution. The traditional Otsu's Thresholding Algorithm (Otsu) can accurately segment infrared images in certain scenarios, but its segmentation performance is limited when dealing with multi-level or complex images, making it prone to insufficient segmentation. To improve the accuracy of fault area detection in power equipment and compensate for the shortcomings of existing image segmentation algorithms, this study first optimized Otsu and proposed an IIS model. Based on this, further combined with the optimized SSA, an IIS model was constructed.

3.1 Construction of an Infrared Image Segmentation Model Based on Two-Dimensional Otsu Algorithm

Image segmentation targets to subdivide an image into sub regions with significant features and meanings, ensuring a high degree of consistency in the characteristics of each region. Although color image segmentation dominates in most applications, certain specific fields, such as healthcare and industry, still heavily rely on grayscale image segmentation [14]. Especially in the industrial field, IIS usually requires converting color images into grayscale images, using grayscale values to distinguish between targets and backgrounds. The current common image segmentation methods are shown in Fig. 1.

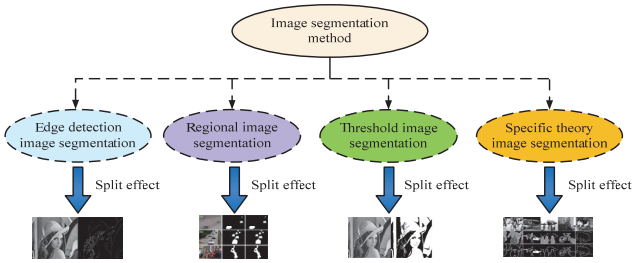

Figure 1 Classification chart of image segmentation methods

In Fig. 1, a total of four image segmentation methods are introduced, namely edge detection, region, threshold, and specific theory image segmentation. Edge detection image segmentation focuses on identifying edges in an image, determining the boundaries of the image by detecting sudden changes in pixel intensity. This method is suitable for situations where there are obvious edges and contrast in the image. The region segmentation method

works by dividing the image into regions with similar attributes, which is usually used in scenes where the differences between regions in the image are obvious but the edges are not clear enough. Threshold image segmentation is the process of dividing pixels in an image into different categories by setting one or more thresholds. Threshold segmentation is suitable for scenes in which the contrast between objects and background in an image is high and can be easily distinguished by brightness or color thresholds. Specific theory image segmentation uses specific theories and algorithms, such as graph theory, fuzzy set theory, or neural networks, to complete complex image segmentation tasks.

Otsu's method, proposed by Nobuyuki Otsu in 1979, is a widely used global threshold algorithm designed to automate the binarization of grayscale images. The main reasons for choosing Otsu algorithm as the basic segmentation method are as follows. The first is that Otsu is able to automatically calculate the optimal threshold without manual intervention to select the threshold. Second, compared to other threshold methods, Otsu shows higher robustness under different brightness and contrast conditions, especially when processing infrared images with uneven illumination. Finally, the Otsu algorithm has relatively low computational complexity and strong adaptability, which is suitable for real-time infrared image segmentation tasks requiring fast response. The basic principle of this algorithm is to find a threshold by statistically analyzing the grayscale distribution of the entire image. This threshold maximizes the inter class variance between the foreground and background of the image, maximizing the difference between them. The probability calculation method for the occurrence of grayscale levels in one-dimensional Otsu is shown in Eq. (1).

$$p_i = \frac{n_i}{N} \quad i = 0,1,2,\cdots,L-1 \tag{1}$$

In Eq. (1), N means the total amount of pixels in the image. n_i refers to the amount of pixels with grayscale. L indicates the max grayscale level. p_i expresses the probability of occurrence of grayscale i. The expression for calculating the mean grayscale of the entire image is shown in Eq. (2) [15, 16].

$$u_T = \sum_{i=0}^{L-1} ip_i \tag{2}$$

In Eq. (2), u_T represents the mean grayscale. Dividing the pixels of the entire image into C_0 and C_1 parts can obtain the grayscale mean of C_0, as shown in Eq. (3).

$$u_0 = \sum_{i=0}^{T} \frac{ip_i}{w_0} \tag{3}$$

In Eq. (3), u_0 represents the grayscale mean of C_0. w_0 represents the variance of C_0. The average grayscale of C_1 is shown in Eq. (4).

$$u_1 = \sum_{i=T+1}^{L-1} \frac{ip_i}{w_1} \tag{4}$$

In Eq. (4), u_1 represents the grayscale mean of C_1. w_1 represents the variance of C_1. The range of values for the C_0 and C_1 grayscale ranges is shown in Eq. (5).

$$\begin{cases} C_0 \in [0,T] \\ C_1 \in [T+1, L-1] \end{cases} \tag{5}$$

In Eq. (5), $[0,T]$ and $[T+1,L-1]$ represent the grayscale ranges of C_0 and C_1, respectively. The calculation for inter class variance can be obtained by combining Eqs. (1) to (5), as shown in Eq. (6).

$$\sigma^2 = w_0 w_1 (u_0 - u_1)^2 \tag{6}$$

In Eq. (6), σ^2 represents the maximum inter class variance. On the basis of one-dimensional Otsu, further expanding the grayscale information of the pixel neighborhood can obtain the probability of the occurrence of pixels in two-dimensional Otsu with a grayscale of i and an average grayscale of j in the neighborhood, as shown in Eq. (7).

$$p_{ij} = \frac{n_{ij}}{\sum_{i=0}^{L-1}\sum_{j=0}^{L-1} n_{ij}} \tag{7}$$

In Eq. (7), p_{ij} denotes the probability of pixels with a grayscale of i and a neighborhood average grayscale of j appearing in the entire image. n_{ij} indicates the amount of pixels with a grayscale of i and a neighborhood average grayscale of j. Assuming (s_1,t_1) and (s_2,t_2) are thresholds in two sets of two-dimensional Otsu, the threshold histogram of two-dimensional Otsu is obtained as shown in Fig. 2.

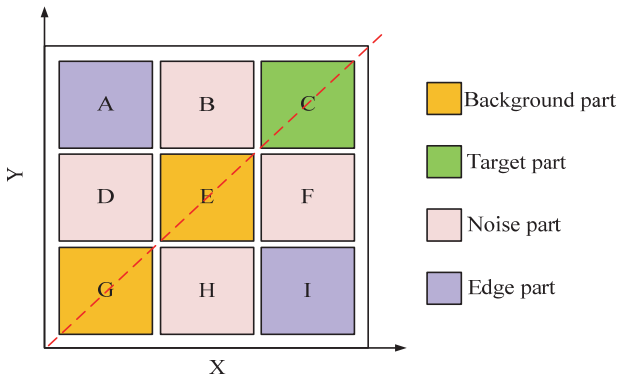

Figure 2 Histogram of 2D Otsu thresholds

In Fig. 2, the threshold histogram of two-dimensional Otsu is mainly divided into nine parts. Among them, G and E can be used as the background part, C can be used as the target part, and A, B, D, F, H, and I are the edge part and noise part. It sets the region probabilities of background parts G, E, and target parts C to ω_0, SS ω_1, and ω_2,

respectively, and obtains the mean values of G, E, and C as μ_0, μ_1, and μ_2, respectively. The mean values of IIS under the two-dimensional Otsu algorithm are shown in Eq. (8).

$$\mu_T = \left(\sum_{i=0}^{L} \sum_{j=0}^{L} (i-1)\, p_{ij}, \sum_{i=1}^{L} \sum_{j=1}^{L} (j-1) p_{ij} \right)^{\tau} \tag{8}$$

In Eq. (8), μ_T represents the mean of the entire image in the segmentation model. τ represents the threshold. According to Eq. (8), the maximum inter class variance functions of (s_1, t_1) and (s_2, t_2) are obtained as shown in Eq. (9).

$$\delta = \omega_0 \lambda_0 + \omega_1 \lambda_1 + \omega_2 \lambda_2 \tag{9}$$

In Eq. (9), δ represents the maximum inter class variance function. λ_0, λ_1, and λ_2 represent the inter class variance coefficients of G, E, and C, respectively. The calculation for λ_0 is shown in Eq. (10).

$$\lambda_0 = \left(\mu_{0,i} - \mu_{T,i} \right)^2 + \left(\mu_{0,j} - \mu_{T,j} \right)^2 \tag{10}$$

In Eq. (10), $\mu_{0,i}$ expresses the mean of *i* appearing in the G part. $\mu_{0,j}$ denotes the mean of *j* appearing in the G part. $\mu_{T,i}$ and $\mu_{T,j}$ represent the mean of *i* and *j* appearing in the entire image, respectively. The calculation for λ_1 is indicated in Eq. (11).

$$\lambda_1 = \left(\mu_{1,i} - \mu_{T,i} \right)^2 + \left(\mu_{1,j} - \mu_{T,j} \right)^2 \tag{11}$$

In Eq. (10), $\mu_{1,i}$ denotes the mean of *i* appearing in E. $\mu_{1,j}$ refers to the mean of *j* appearing in E. The calculation for λ_2 is denoted in Eq. (12).

$$\lambda_2 = \left(\mu_{2,i} - \mu_{T,i} \right)^2 + \left(\mu_{2,j} - \mu_{T,j} \right)^2 \tag{12}$$

In Eq. (12), $\mu_{2,i}$ indicates the mean of *i* appearing in C. $\mu_{2,j}$ represents the mean of *j* appearing in C.

3.2 Design of Image Segmentation Algorithm Based on Variable Helix Optimized-Sparrow Search Algorithm

To achieve better segmentation results, higher image processing efficiency, and better display of the feature details of infrared images in the two-dimensional Otsu algorithm-based IIS model, a VHO-SSA was further proposed to optimize the maximum inter class variance function in the IIS model. Traditional SSA is a swarm based optimization algorithm, which is simple and efficient, but it is easy to fall into local optimal solutions when dealing with complex or multi-modal optimization problems, especially when the search space is extensive and irregular. In addition, the convergence rate of SSA may be slow in high-dimensional search Spaces, especially when the optimization objective function is extremely complex. At the same time, traditional SSA mainly relies on random behavior to update the sparrow's position, which may lead to insufficient search efficiency, especially in the application scenarios requiring fine search. In order to overcome these limitations of traditional SSA, variable spiral position search method and optimal point set method are introduced to optimize, and VHO-SSA is proposed. The variable spiral position search method is inspired by the hunting behavior of whales in nature. By dynamically adjusting the search strategy by simulating spiral diving, the search space can be explored and utilized more effectively. By improving the initial distribution of the population, the optimal point set method can cover the entire search space more evenly, thus improving the convergence speed and stability of the algorithm. It can be seen that the variable spiral method can increase the global search ability of the algorithm, effectively avoid the local optimal trap, and improve the search efficiency of SSA in complex environments. The optimal point set can optimize the initial solution set of SSA, improve the global exploration ability, and help the algorithm to better locate the potential global optimal solution in the initial stage.

In the two-dimensional Otsu IIS problem, due to the fact that the information contained in the segmentation model far exceeds that of the one-dimensional Otsu segmentation model, the study introduced VHO-SSA to optimize the maximum inter class variance function value, aiming to raise the running speed of the model and optimize its image segmentation effect [16, 17]. Fig. 3 expresses the traditional SSA running flowchart.

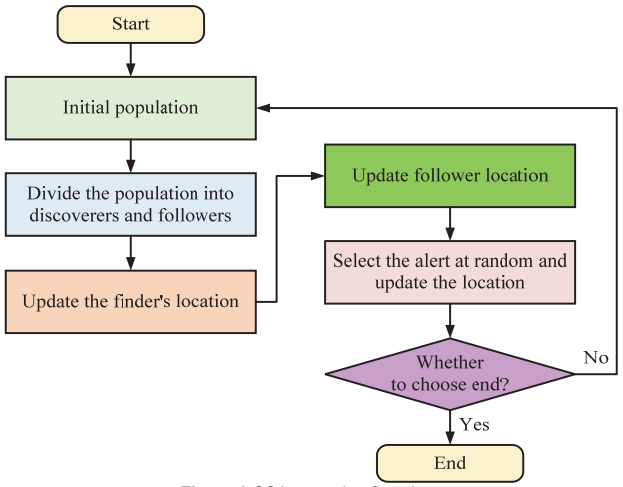

Figure 3 SSA operation flowchart

Fig. 3 shows the operational process of traditional SSA. The population in SSA is composed of discoverers and followers, with a relationship of opposition and unity between discoverers and followers. The discoverer is responsible for searching for food, providing foraging areas and directions for followers. Followers monitor discoverers and can become new discoverers through competition. In addition to discoverers and followers, there is also a special type of early warning system that can warn of danger and alert, ensuring that the population is in a safe area. With the early warning personnel, the local search

space in SSA can be well developed. Although SSA has the above advantages, it still has issues such as not quick convergence speed and insufficient accuracy. Therefore, to improve the image segmentation's accuracy, the variable helix position search method (VHPSM) was introduced to optimize SSA. The VHPSM originates from the helix predation concept in whale algorithms. By using the VHPSM, the follower's position can be made more flexible, thereby developing more optimized paths. The path search diagram of the VHPSM is illustrated in Fig. 4.

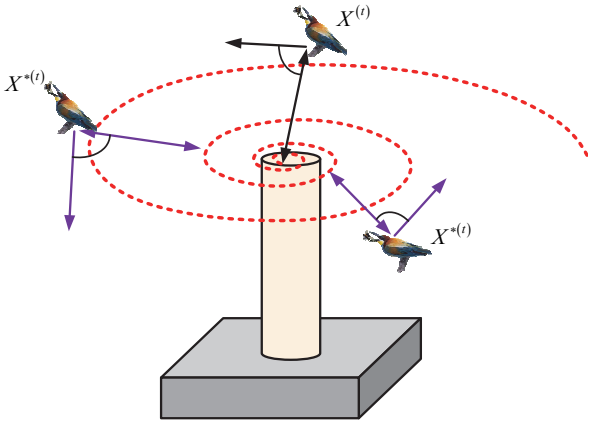

Figure 4 Path helix search diagram

In Fig. 4, $X^{(t)}$ and $X^{*(t)}$ represent the original position of the follower and the changed position after introducing the VHPSM, respectively. The VHPSM comes from the whale algorithm, and the whale in the whale algorithm not only has the ability to perform random search, but also has the ability to helix upstream and bubble predation. Therefore, in the VHPSM, when the follower updates the position using bubbles, the position update formula shown in Eq. (13) is obtained [18-20].

$$X_i^{t+1} = \left| X_{\text{best}}^t - X_i^t \right| \cdot e^{zl} \cdot \cos(2\pi l) + X_{\text{best}}^t \tag{13}$$

In Eq. (13), X_i^{t+1} represents the position of the follower with grayscale i at time $t+1$. X_{best}^t represents the optimal position at t time. X_i^t represents the position of followers with grayscale i at t time. e represents the cardinality of natural logarithms. z represents the parameter. l represents a constant. To improve the global search capability of SSA, further optimization of parameter z was studied, which was set as an adaptive parameter. The calculation for NN is shown in Eq. (14).

$$z = e^{k \cdot \cos\left(\pi \cdot \left(1 - \frac{t}{M}\right)\right)} \tag{14}$$

In Eq. (14), k represents the dimension. M represents the number of position updates. In addition to using the VHPSM to optimize the position of followers, the study also optimized the initial sparrow population using a set of good points, making it as evenly distributed as possible to avoid the initial population not being able to cover all solutions. In the set of optimal points, assuming G_s is a cube, the set of points is $r = \{r_1, r_2, ..., r_s\}$, and the elements in the set are $r_k = \left\{ 2\cos\frac{2\pi k}{p},\ 1 \le k \le s \right\}$. The expression of the best point set is shown in Eq. (15).

$$p_n(i) = \left\{ \{r_1 \times i\}, \{r_2 \times i\}, ..., \{r_s \times i\},\ i = 1, 2, ..., n \right\} \tag{15}$$

In Eq. (15), $p_n(i)$ represents the set of best points. The deviation expression for the set of good points is shown in Eq. (16).

$$\phi(n) = C(r, \varepsilon) n^{-1+\varepsilon} \tag{16}$$

In Eq. (16), ε represents any small constant, $C(r, \varepsilon)$ represents a constant related to r, ε, and $p_n(i)$ is the optimal set. It assumes that a sparrow population with a size of 20 is distributed in a square area, the results of initializing the population distribution with random distribution and optimal point set are expressed in Fig. 5.

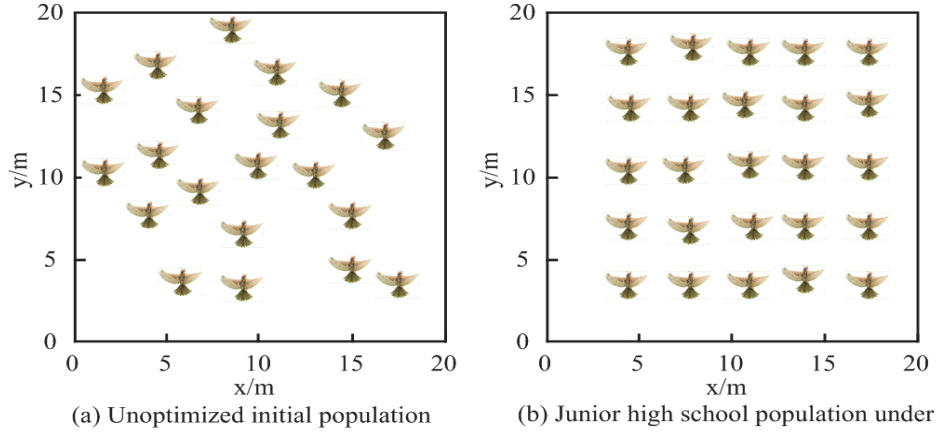

(a) Unoptimized initial population

(b) Junior high school population under optimal point set optimization

Figure 5 Initial distribution of sparrow population

From Fig. 5, compared to ordinary random distributions, the initial population distribution of the best point set is more uniform and covers space more comprehensively. Therefore, using a good point set can further improve the traversal of the SSA search space. Using the maximum inter class variance function in Eq. (9)

as the fitness function, the VHPSM and the optimized SSA of the best point set are used to optimize the parameters in this function, and the final image segmentation result value is obtained. Based on the above optimization schemes, the operational flowchart of VHO-SSA for segmenting infrared images is shown in Fig. 6.

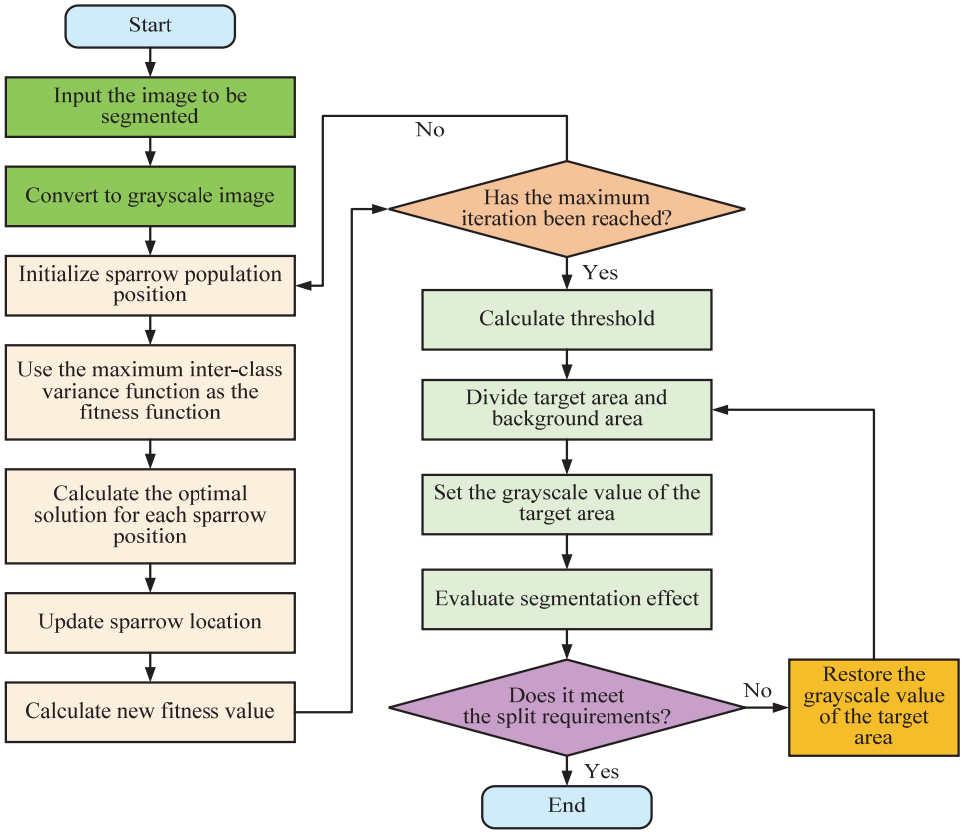

Figure 6 Flowchart of VHO-SSA algorithm operation

Fig. 6 shows the running process of the VHO-SSA. Firstly, the image was input to be segmented and converted into a grayscale image. Then, the initial position of the sparrow population was optimized using the VHPSM and the best point set method. Then, using the maximum inter class variance function as the fitness function, the optimal position of sparrow individuals was calculated. According to the variable helix improvement strategy, it optimized the position of sparrows and calculated new fitness values. If the maximum iteration was reached at this point, the VHO-SSA optimization results were utilized to calculate the threshold and divide the target area and background area. After setting the grayscale value of the target area, the optimized segmented image was evaluated using the intersection union ratio evaluation index. If the segmentation requirements were met, the output image was segmented. If not, the algorithm parameters needed to be readjusted to continue optimizing.

4 TEST RESULTS OF INFRARED IMAGE SEGMENTATION MODEL BASED ON IMPROVED SSA

To test the performance of VHO-SSA, the experiment used the publicly available infrared image dataset IRIS, which contains 500 infrared images under different scenarios, covering multiple application scenarios such as industrial equipment detection and natural environment monitoring. All images have a resolution of 640 × 480 pixels and are taken by professional infrared imaging equipment under different lighting and temperature conditions. In order to comprehensively evaluate the performance of the proposed algorithm, the Structural Similarity Index Measure (SSIM) is used to evaluate the visual similarity between the segmented image and the original image. The Peak Signal-to-Noise Ratio (PSNR) was used to evaluate the degree of information loss during image segmentation, and the accuracy, recall rate and F1 score were also calculated to quantify the accuracy and completeness of segmentation. SSIM is chosen because it can reflect the structural information retention of the image, while PSNR can reflect the degree of image quality loss. Together, these indicators can comprehensively evaluate the ability of image segmentation algorithms to preserve detail and suppress noise.

4.1 VHO-SSA Segmentation Performance Testing

In order to comprehensively evaluate the performance of the optimization algorithm in different types of image segmentation tasks, five benchmark functions, Sphere, Rosenbrock, Rastrigin, Ackley and Griewank, were selected for testing. These functions have different characteristics, such as single-peak and multi-peak functions, so as to simulate various complex situations that may be encountered in practical image segmentation. In addition, VHO-SSA was compared with traditional SSA, Whale Optimization Algorithm (WOA), and Differential Evolution-Sparrow Search Algorithm (DE-SSA). Multiple experiments were conducted on each function and the results of each experiment were recorded. To ensure the

stability of the experiment, all simulation tests were conducted using the same computer equipment in the same environment, as shown in Tab. 1.

Table 1 Computer equipment information

Name	Configuration
Video card	GTX 1080ti
CPU	Inter Xeon E5
Gpu-accelerated library	CUDA 10.0
Memory	64 GB
Operating system	Windows 10
Deep learning framework	TensorFlow 1.8

Tab. 1 provides a detailed description of the operating system, memory size, central processing unit, and other configurations of the computers used. For the involved different methods, the same population size and iteration times were set, and each method was run separately. In VHO-SSA, the population size is set to 50, which is based on the optimal value determined after the initial test comparison, to ensure that the algorithm has sufficient search power and good computational complexity. The number of iterations is usually set to 100, which is enough for the algorithm to converge in most cases. The spiral update coefficient is the key parameter introduced in this algorithm. Through the parameter sensitivity analysis of the system, it can be observed that when the spiral update coefficient increases from 0.2 to 0.8, the segmentation accuracy of the algorithm gradually improves, but the segmentation time increases significantly when the spiral update coefficient exceeds 0.5. It can be seen that the spiral update coefficient has a decisive influence on the performance balance of the algorithm, and its final value is set to 0.5, which is used to control the spiral tightness of the search path. Firstly, the mean convergence curves of each algorithm in unimodal and multimodal functions were evaluated, as shown in Fig. 7.

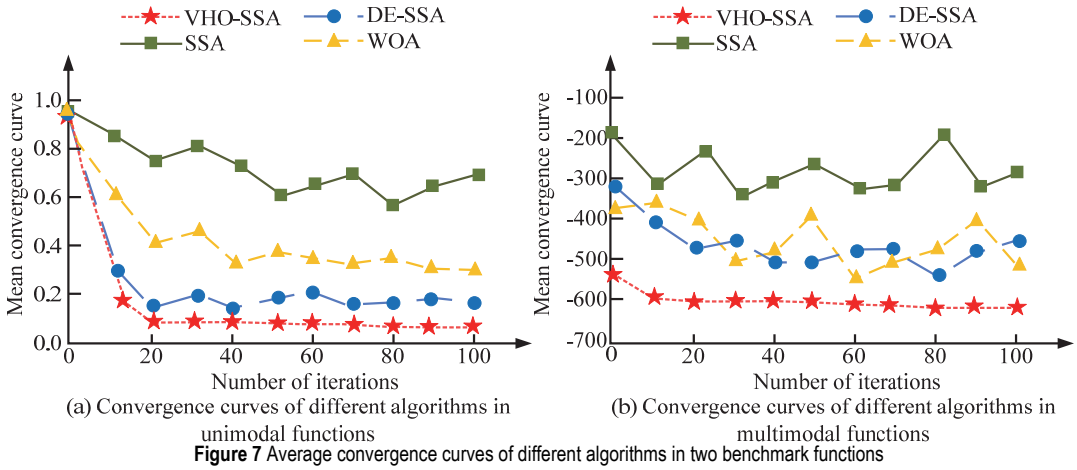

Figure 7 Average convergence curves of different algorithms in two benchmark functions

Figs. 7a and 7b show the average convergence curves of SSA, WOA, DE-SSA, and VHO-SSA in unimodal and multimodal functions, respectively. From Fig. 7a, as the iteration times increased, the mean convergence curves of the four algorithms in the unimodal function all showed a downward trend. However, VHO-SSA could reach a stable state when iterated to around 20 generations, while SSA, WOA, and DE-SSA would continue to fluctuate. From Fig. 7b, as the number of iterations increased, the average convergence curve of VHO-SSA in multimodal functions was generally stable, but SSA, WOA, and DE-SSA would continue to exhibit significant fluctuations. When the number of iterations was 11, VHO-SSA could reach a stable state in a multimodal function.

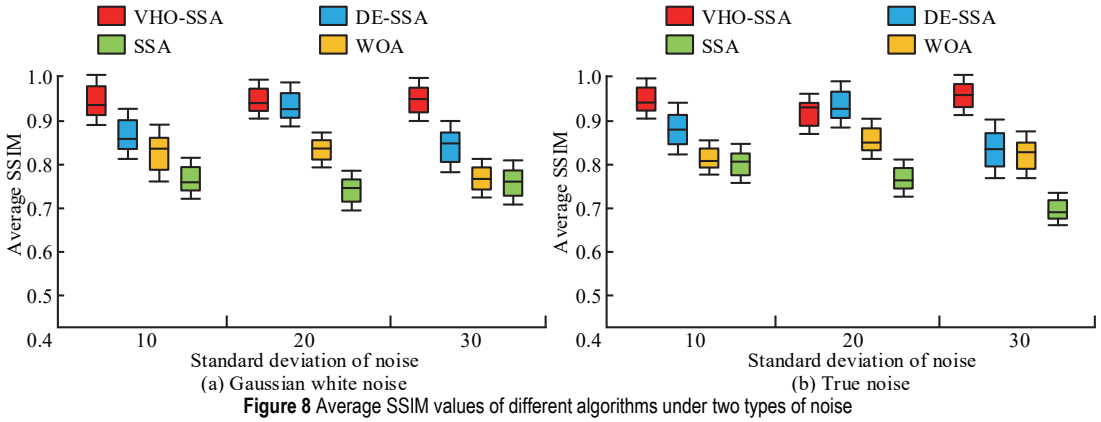

Figure 8 Average SSIM values of different algorithms under two types of noise

Figs. 8a and 8b show the average SSIM of SSA, WOA, DE-SSA, and VHO-SSA under Gaussian white noise and real noise, respectively. Combining Figs. 8a and 8b, when the noise standard deviation was within the range of 10 dB~30 dB, the SSIM values of VHO-SSA, DE-SSA, WOA, and SSA under Gaussian white noise and real noise were always above 0.90, between 0.80~0.95, between 0.75~0.85, and between 0.65~0.80, respectively. The SSIM value of VHO-SSA was closest to 1, so the denoising effect of this algorithm was better.

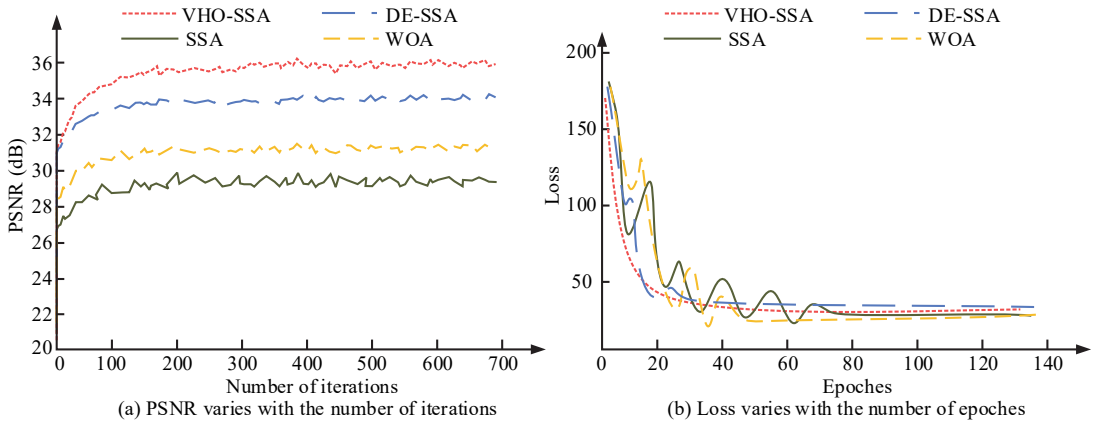

(a) PSNR varies with the number of iterations (b) Loss varies with the number of epoches

Figure 9 PSNR values and Loss values for different algorithms

Figs. 9a and 9b show the changes in PSNR and loss values of SSA, WOA, DE-SSA, and VHO-SSA, respectively. According to Fig. 9a, as the number of iterations increased, the PSNR values of all four algorithms increased. The maximum PSNR values of SSA, WOA, DE-SSA, and VHO-SSA in stable state were 29.1, 30.8, 33.7, and 35.9, respectively. In Fig. 9b, when the number of iterations was 74, 48, 25, and 19, SSA, WOA, DE-SSA, and VHO-SSA could obtain stable loss functions. Compared to the other three algorithms, VHO-SSA could iterate to a stable state faster, thus having a faster image processing speed.

4.2 Analysis of Application Effects of Infrared Image Segmentation Models

In addition to verifying the performance of each segmentation algorithm, the study further applied each segmentation algorithm to practical IIS tasks. Three different infrared images were selected as reference samples, and the segmentation results of SSA, DE-SSA, and VHO-SSA segmentation algorithms in actual IIS problems are shown in Fig. 10.

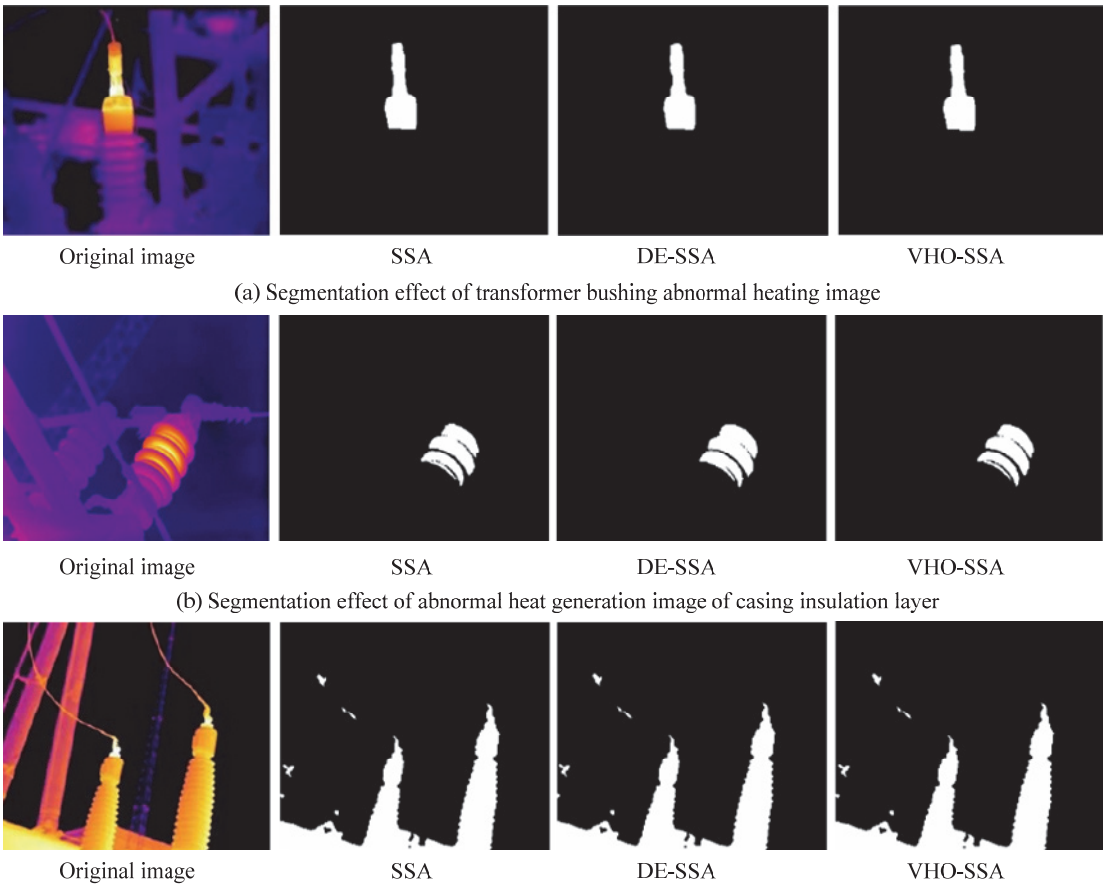

(a) Segmentation effect of transformer bushing abnormal heating image

(b) Segmentation effect of abnormal heat generation image of casing insulation layer

(c) Segmentation effect of breaker connector fault image

Figure 10 Actual segmentation effect of different infrared images under different algorithms

Three different infrared images were selected in Fig. 10 to test the effectiveness of each algorithm model in actual segmentation tasks. Figs. 10a, b, and c show the infrared images of abnormal heating of the transformer bushing, the infrared images of abnormal heating of the insulation layer of the bushing, and the infrared images of

the fault heating of the high-voltage side tube circuit breaker joint, respectively. Based on Figs. 10a, b, and c, VHO-SSA can achieve good segmentation results in three different infrared images, with clearer segmentation edges and better presentation of segmentation details.

Table 2 Computer equipment information

Infrared image type	Segmentation model	Segmentation accuracy	MSE	Time
Transformer bushing abnormal heat	SSA	0.82	26.54	16.4s
	DE-SSA	0.93	18.28	8.3s
	VHO-SSA	0.97	3.16	3.6s
Abnormal heating of bushing insulation layer	SSA	0.78	35.47	21.8s
	DE-SSA	0.89	22.52	11.6s
	VHO-SSA	0.98	5.21	1.2s
Faulty heating of tube breaker connector on high-voltage side	SSA	0.81	32.45	19.7s
	DE-SSA	0.90	20.09	9.1s
	VHO-SSA	0.96	2.37	2.9s

Tab. 2 shows the segmentation accuracy, MSE, and segmentation time of SSA, DE-SSA, and VHO-SSA segmentation models in three types of infrared images. According to Tab. 2, the segmentation accuracy of VHO-SSA in all three types of infrared images was above 0.95, with the highest reaching 0.98. The segmentation time was all within 5 seconds, with a minimum of only 1.2 seconds. In addition, the MSE value of its image segmentation was much lower than SSA and DE-SSA, with a minimum of only 2.37. The infrared segmentation model optimized by VHO-SSA could achieve good performance in actual segmentation tasks.

In order to verify the superiority of the proposed method, ANOVA test was also used to analyze whether the results of different algorithms on multiple performance indicators were statistically significant. The results of segmentation accuracy, MSE and segmentation time of different algorithms shown in Tab. 2 were tested by ANOVA, and it was found that the differences between the proposed VHO-SSA algorithm and other algorithms in segmentation accuracy and MSE reached a statistically significant level ($P < 0.05$). The reason for the significant difference is that VHO-SSA algorithm shows higher segmentation accuracy when processing low-contrast images, which is mainly due to its variable spiral search strategy, which improves the search ability and adaptability of the algorithm in complex image background. Although VHO-SSA showed superiority in most of the tests, in extremely noisy images, traditional SSA had an advantage in computation time due to its simplified search mechanism. This suggests that a simplified version of SSA may be more suitable for applications that require very high real-time performance.

Table 3 Comparison of segmentation effects of four advanced algorithms

Segmentation model	Segmentation accuracy	Computational complexity	Robustness
U-Net	0.89	0.25	High noise decreased by 89.12%
DeepLab	0.91	0.18	High noise decreased by 91.56
FCN	0.93	0.12	High noise decreased by 95.72%
VHO-SSA	0.98	0.03	High noise decreased by 96.35%

Tab. 3 shows the changes of segmentation accuracy, computational complexity and robustness of four advanced image segmentation algorithms U-Net, DeepLab, FCN and VHO-SSA under high noise environment. As can be seen from Tab. 3, the segmentation accuracy of VHO-SSA in high-noise environment is the highest, up to 0.98. In addition, its computational complexity and robustness are also the best, with the computational complexity as low as 0.03, while the robustness can be reduced by 96.35% in high-noise environment.

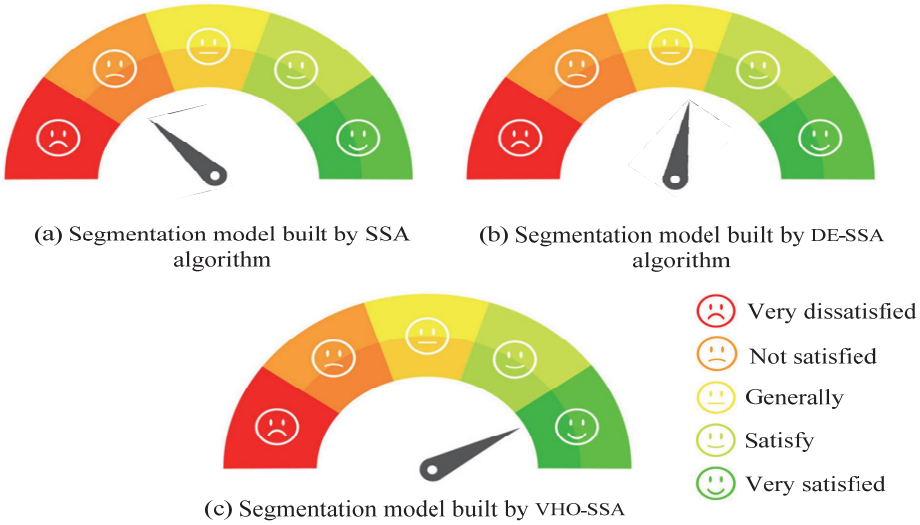

(a) Segmentation model built by SSA algorithm

(b) Segmentation model built by DE-SSA algorithm

(c) Segmentation model built by VHO-SSA algorithm

Figure 11 Plot of experts' satisfaction scores for different segmentation models

Figs. 11a, b, and c show the satisfaction of 15 experts with the segmentation performance of SSA, DE-SSA, and VHO-SSA segmentation models, respectively. According to Fig. 11, the 15 experts showed the highest satisfaction with the segmentation of the VHO-SSA model, while the satisfaction with the segmentation of the other two models was relatively low.

5 CONCLUSION

In conclusion, this study proposes a novel infrared image segmentation method based on a Variable Helix Optimized-Sparrow Search Algorithm (VHO-SSA). The proposed method combines the Otsu threshold algorithm with an optimized sparrow search algorithm, which utilizes a variable helix position search method and a best point set method to improve segmentation performance. The experimental results demonstrate that VHO-SSA outperforms other state-of-the-art algorithms in terms of segmentation accuracy, structural similarity, and noise resilience. The proposed method shows promise for improving the segmentation of infrared images in various applications, such as security monitoring, remote sensing imaging, and clinical medicine. However, further research is needed to evaluate the performance of VHO-SSA on large-scale datasets and high-resolution images and to explore its practical implications for real-world applications. Additionally, the limitations of the current study, such as the choice of benchmark functions and evaluation metrics, should be addressed in future research to provide a more comprehensive assessment of the proposed method.

6 REFERENCES

[1] Tang, Y., Dai, Q., Yang, M., Du, T., & Chen, L. (2023). Software defect prediction ensemble learning algorithm based on adaptive variable sparrow search algorithm. *International Journal of Machine Learning and Cybernetics*, *14*(6), 1967-1987. https://doi.org/10.1007/s13042-022-01740-2

[2] Jiang, J., Bie, Y., Li, J., Yang, X., Ma, G., Lu, Y., & Zhang, C. (2021). Fault diagnosis of the bushing infrared images based on mask R-CNN and improved PCNN joint algorithm. *High voltage*, *6*(1), 116-124. https://doi.org/10.1049/hve.2019.0249

[3] Nyo, M. T., Mebarek-Oudina, F., Hlaing, S. S., & Khan, N. A. (2022). Otsu's thresholding technique for MRI image brain tumor segmentation. *Multimedia tools and applications*, *81*(30), 43837-43849. https://doi.org/10.1007/s11042-022-13215-1

[4] Wang, W., Tu, A., & Bergholm, F. (2022). Improved minimum spanning tree based image segmentation with guided matting. *KSII Transactions on Internet and Information Systems (TIIS)*, *16*(1), 211-230. https://doi.org/10.3837/tiis.2022.01.012

[5] Abualigah, L., Almotairi, K. H., & Elaziz, M. A. (2023). Multilevel thresholding image segmentation using meta-heuristic optimization algorithms: Comparative analysis, open challenges and new trends. *Applied Intelligence, 53*(10), 11654-11704. https://doi.org/10.1007/s10489-022-04064-4

[6] Luo, S., Tai, X. C., & Wang, Y. (2022). A new binary representation method for shape convexity and application to image segmentation. *Analysis and Applications*, *20*(3), 465-481. https://doi.org/10.1142/S0219530521500238

[7] Jiang, Z., He, W., Kirby, M. S., Man, S. A., & Wang, S. (2022). Weakly supervised spatial deep learning for earth image segmentation based on imperfect polyline labels. *ACM Transactions on Intelligent Systems and Technology*, *13*(2), 1-20. https://doi.org/10.1145/3480970

[8] Shuang, Q., Yao, Z., & Shikui, W. (2022). A Survey of Referring Image Segmentation. *Journal of Signal Processing*, *38*(6), 1144-1154.

[9] Xian, S., Cheng, Y., & Chen, K. (2022). A novel weighted spatial T-spherical fuzzy C-means algorithms with bias correction for image segmentation. *International Journal of Intelligent Systems*, *37*(2), 1239-1272. https://doi.org/10.1002/int.22668

[10] Zhang L., Wang C., Fang M., & Xu W. (2022). Spectral Reflectance Reconstruction Based on BP Neural Network and the Improved Sparrow Search Algorithm. *IEICE Transactions on fundamentals of electronics, communications & computer sciences*, *105*(8), 1175-1179. https://doi.org/10.1587/transfun.2021EAL2096

[11] Zhang S., Zhang L., Gai T., Xu P., & Wei Y. (2022). Aberration analysis and compensate method of a BP neural network and sparrow search algorithm in deep ultraviolet lithography. *Applied optics*, *61*(20), 6023-6032. https://doi.org/10.1364/AO.462436

[12] Hui X., Guangbin C., Shengxiu Z., Xiaogang Y., & Mingzhe H. (2022). Hypersonic reentry trajectory optimization by using improved sparrow search algorithm and control parametrization method. *Advances in Space Research: The Official Journal of the Committee on Space Research*, *69*(6), 2512-2524. https://doi.org/10.1016/j.asr.2021.12.030

[13] Liu T., Yuan Z., Wu L., & Badami B. (2021). An optimal brain tumor detection by convolutional neural network and Enhanced Sparrow Search Algorithm. *Proceedings of the Institution of Mechanical Engineers Part H: Journal of Engineering in Medicine*, *235*(4), 459-469. https://doi.org/10.1177/0954411920987964

[14] Fan X., Sun Z., Tian E., Yin Z., & Cao G. (2023). Medical image contrast enhancement based on improved sparrow search algorithm. *International Journal of Imaging Systems and Technology*, *33*(1), 389-402. https://doi.org/10.1002/ima.22794

[15] Xue J., Shen B., & Pan A. (2023). An intensified sparrow search algorithm for solving optimization problems. *Journal of Ambient Intelligence and Humanized Computing*, *14*(7), 9173-9189. https://doi.org/10.1007/s12652-022-04420-9

[16] Gheisari, M., Hamidpour, H., Liu, Y., Saedi, P., Raza, A., Jalili, A., Rokhsati, H., & Amin, R. (2022). Data Mining Techniques for Web Mining: A Survey. *Artificial Intelligence and Applications*, *1*(1), 3-10. https://doi.org/10.47852/bonviewAIA2202290

[17] Carlos de Carvalho, E., Martins Coelho, A., Conci, A., & de Freitas Oliveira Baffa, M. (2023). U-Net Convolutional Neural Networks for breast IR imaging segmentation on frontal and lateral view. *Computer Methods in Biomechanics and Biomedical Engineering: Imaging & Visualization*, *11*(3), 311-316. https://doi.org/10.1080/21681163.2022.2040053

[18] Grewal, R., Kasana, S. S., & Kasana, G. (2023). Hyperspectral image segmentation: a comprehensive survey. *Multimedia Tools and Applications*, *82*(14), 20819-20872. https://doi.org/10.1007/s11042-022-13959-w

[19] Zhou, G., Zhang, Z., Yin, W., Chen, H., Wang, L., Wang, D., & Ma, H. (2024). Surface defect detection of CFRP materials based on infrared thermography and Attention U-Net algorithm. *Nondestructive Testing and Evaluation*, *39*(2), 238-257. https://doi.org/10.1080/10589759.2023.2191954

[20] Huang, X., Yin, C., Dadras, S., Cheng, Y., & Bai, L. (2023). Adaptive rapid defect identification in ECPT based on K-means and automatic segmentation algorithm. *Journal of Ambient Intelligence and Humanized Computing*, *14*(11), 1-18. https://doi.org/10.1007/s12652-017-0671-5

Contact information:

JiLan HUANG, Master degree, Associate Professor
(Corresponding author)
Geely University of China,
641423, ChengDu, China
E-mail: hlhuanglan@163.com

Xing YANG, Associate Professor
Geely University of China,
641423, ChengDu, China
E-mail: 18980091368@163.com

ZhiXiong JIN, Bachelor degree, Associate Professor
Geely University of China,
641423, ChengDu, China
E-mail: jinzhixiong@hongyicg.com